In vivo MR spectroscopy reflects synapse density in a Huntington's disease mouse model

Nicole Zarate[1*], Katherine Gundry[2*], Dahyun Yu[1], Jordan Casby[3], Lynn E Eberly[4,2], Gülin Öz[2] and Rocio Gomez-Pastor[1].

[1]Department of Neuroscience, School of Medicine, University of Minnesota, Minneapolis, MN, United States. [2]Center for Magnetic Resonance Research, Department of Radiology, School of Medicine, University of Minnesota, Minneapolis, MN, United States. [3]Department of Pharmacology, School of Medicine, University of Minnesota, Minneapolis, MN, United States. [4]Division of Biostatistics, School of Public Health, University of Minnesota, Minneapolis, Minnesota.

[*]These authors contributed equally to the manuscript

ORCiD: Nicole Zarate (0000-0003-4839-7783), Katie Gundry (0000-0002-3333-1709), Dahyun Yu (0000-0002-3179-4080), Jordan Casby (0000-0002-5601-3906), Lynn Eberly (0000-0003-4763-330X), Gülin Öz (0000-0002-5769-183X), Rocio Gomez-Pastor (0000-0003-1136-5462)

± Correspondence should be addressed to Rocio Gomez-Pastor, University of Minnesota, 321 Church St. SE, Jackson Hall Room 6-145, Minneapolis, MN 55455, rgomezpa@umn.edu

Word Count (5000): 4984

Relevant conflicts of interest/Financial Disclosure: Nothing to report

Funding Sources: This work was supported by the University of Minnesota Biomedical Research Awards for Interdisciplinary New Science (to R.G.P and G.O) and the National Institute of Health NINDS (R01 NS110694) (to R.G.P). The Center for Magnetic Resonance Research is supported by the National Institute of Biomedical Imaging and Bioengineering (NIBIB) grant P41 EB027061, the Institutional Center Cores for Advanced Neuroimaging award P30 NS076408 and the W.M. Keck Foundation.

Keywords: Huntington's disease, zQ175, synapse density, ^{1}H-MRS, CK2 alpha prime, neurochemicals, biomarkers.

Abstract (250 Words)

Background: Striatal medium spiny neurons are highly susceptible in Huntington's disease (HD), resulting in early synaptic perturbations that lead to neuronal dysfunction and death. Non-invasive imaging techniques, such as proton magnetic resonance spectroscopy (^{1}H-MRS), have been used in HD mouse models and patients with HD to monitor neurochemical changes associated with neuronal health. However, the molecular connection between brain neurochemical alterations and synaptic dysregulation is unknown, limiting our ability to monitor potential treatments that may affect synapse function.

Objective: Assess the intersection of synapse density and ^{1}H-MRS during disease progression in an HD mouse model.

Methods: We conducted *in vivo* longitudinal ^{1}H-MRS in the striatum followed by *ex-vivo* analyses of excitatory synapse density of two synaptic circuits disrupted in HD: thalamo-striatal (T-S) and cortico-striatal (C-S) pathways. We used the heterozygous knock-in zQ175 HD mouse model as well as zQ175 mice lacking one allele of CK2α'(zQ175$^{(Tg/0)}$:CK2α'$^{(+/-)}$), a kinase previously shown to regulate synapse function in HD.

Results: Longitudinal analyses of excitatory synapse density showed early and sustained reduction in T-S synapses in zQ175 mice, preceding C-S synapse depletion, which was rescued in zQ175:CK2α'$^{(+/-)}$. Linear regression analyses showed C-S synapse number correlated with ^{1}H-MRS-measured levels of GABA while T-S synapse number positively correlated with alterations in the levels of alanine, phosphoethanolamine, lactate, and taurine relative to total creatine.

Conclusion: We propose these neurochemicals could be used as surrogate biomarkers to monitor circuit-specific synaptic dysfunction using ^{1}H-MRS in the zQ175 mouse model and perhaps in HD pre-clinical studies.

INTRODUCTION

Huntington's disease (HD) is an autosomal dominant, neurodegenerative disorder caused by expansion of a trinucleotide repeat (CAG) in exon 1 of the Huntingtin gene (*HTT)*[1]. This expansion results in a poly-glutamine (polyQ) containing mutant form of the HTT protein (mHTT) that is prone to misfolding and aggregation. mHTT aggregation occurs in virtually all cell types in the body but preferentially affects medium spiny neurons (MSN) of the striatum, causing striatal synaptic perturbations and neuronal death. HD is characterized by progressive motor, cognitive, and psychiatric deficits for which there is no cure or effective therapies. To design therapies that effectively modify disease symptoms it is necessary to identify robust HD biomarkers able to objectively monitor disease onset and progression.

Mouse models of HD and patients with prodromal HD show perturbations in striatal synaptic stability and functional connectivity, respectively, before motor symptom onset or overt neuronal cell death[2,3]. MSNs receive excitatory glutamatergic input from the cortex and intralaminar nuclei of the thalamus and both D1 and D2-type MSNs rely equally on these excitatory inputs[4,5]. Dysfunction in the cortico-striatal (C-S) pathway has been widely reported in HD, showing that disruptions in this circuitry occur prior to MSN death thereby suggesting they are the leading cause for neuronal dysfunction[2,3,6]. However, recent studies in cells and mouse models of HD showed that thalamic input is also disrupted in HD and occurs before C-S circuit pathology or onset of motor symptoms[6–9] indicating that the thalamo-striatal (T-S) excitatory circuit may play a more prominent role in early HD pathogenesis than previously thought. In support of these studies, depletion of Protein Kinase CK2α', a kinase involved in protein homeostasis and neuroinflammation, in the heterozygous zQ175 HD mouse model ameliorated early T-S synapse loss and long-term HD-like symptoms with limited impact on C-S synapse density[8]. Altogether, these data suggest that monitoring synapse density could be used as a potential HD biomarker.

In vivo monitoring of synapses in the human brain imposes a significant technical challenge. Positron emission tomography (PET) with radioligands targeting various synaptic vesicle proteins can be used to monitor synaptic density in both animals and humans[10,11]. However, the limited availability of these PET tracers and concerns about repeated radiation exposure provide motivation to assess alternative neuroimaging technologies to evaluate synapse density. Magnetic resonance (MR) methods like functional MR imaging (fMRI) and MR spectroscopy (MRS) overcome these concerns but have yet to be evaluated as markers of synaptic density. MRS has recently emerged as a useful tool to evaluate neurochemical alterations in HD and other polyQ diseases[12–15]. Studies in various mouse models of HD and in patients with HD have highlighted consistent alterations in key neurochemicals that can be associated with neurodegeneration, such as depletion of the neuronal integrity marker N-acetyl aspartate (NAA) or increased levels of the putative gliosis marker myo-inositol (Ins)[16–18, 19]. However, the molecular mechanism that connects brain neurochemical changes with functional decline is still unknown, limiting our understanding of how potential treatments that may affect synapse function translate into alterations of brain metabolites. Previous studies in patients with different spinocerebellar ataxias

presenting different degrees of synapse loss proposed that neurochemical alterations measured by MRS may reflect changes in synaptic function or density[14,21]. Consistently, a recent MRS study in aged zQ175 mice showed that key striatal neurochemical alterations paralleled changes in T-S synapses[22], highlighting the potential use of MRS as a tool to monitor synapse density. However, the relationship between neurochemical alterations and synaptic density has not been directly assessed thus far.

In the present study we conducted *in vivo* longitudinal high field proton (^{1}H) MRS in the striatum followed by *ex-vivo* analyses of T-S and C-S excitatory synapse densities in the heterozygous zQ175 HD mouse model and in zQ175 mice lacking one allele of CK2α'. We found that T-S synaptic density was significantly correlated with alterations in a multitude of neurochemicals including Ala, Lac, PE, and Tau/tCr while C-S synapse number significantly correlated with GABA. We propose that GABA, Ala, Lac, PE, and tau/tCr alterations could be used as surrogate biomarkers to monitor circuit-dependent synapse dysfunction during HD in zQ175 mice. Furthermore, these results support using MRS as a technique in future HD pre-clinical studies to monitor treatment efficacy in altering excitatory synaptic function in the striatum.

METHODS

Animal Preparation for MR Scanning

All experiments were performed according to procedures approved by the University of Minnesota Institutional Animal Care and Use Committee. We selected three time points based on progression of motor symptoms[17,34]: 3 months (pre-symptomatic), 6 months (early symptomatic) and 12 months (symptomatic). Longitudinal neuroimaging provided information for how neurochemical levels changed within individual mice over time. Animals were induced with 3% isoflurane in a 1:1 mixture of O_2:N_2O. Mice were secured in a custom-built mouse holder and physiological status was monitored (SA Instruments) and recorded. Anesthesia was maintained with 1.5-2% isoflurane to achieve a respiration rate of 70-100 breaths per minute. Body temperature was maintained at 36-37ºC with a circulating warm water system and a heating fan controlled by feedback received from a fiber-optic rectal thermometer. The scan session was approximately 50 minutes for each animal. A large cohort of mice (WT n=13, zQ175 n=16, and zQ175:CK2α'$^{(+/-)}$ n=16) were scanned at 3 months using a 9.4T scanner, after which a subset of the animals (n=4 per genotype) were sacrificed for the 3 month time point for synapse density analyses. Remaining animals were aged to 6 months at which time they were again scanned (WT n=9, zQ175 n=12, and zQ175:CK2α'$^{(+/-)}$ n=13), and a small cohort (n=4 animals per genotype) sacrificed for synapse density. Two zQ175:CK2α'$^{(+/-)}$ mice were sacrificed prior to being scanned at 12 months due to health issues. The remaining animals (WT n=5, zQ175 n=8, and zQ175:CK2α'$^{(+/-)}$ n=7) were scanned at 12 months followed by striatal synapse density analyses.

MR Protocol

All experiments were performed on a 9.4T/31 cm scanner (Agilent), as described previously[23,24]. A quadrature surface radio frequency (RF) coil with two geometrically decoupled single turn coils (14 mm diameter) was used as the MR transceiver. Following positioning of the mouse in the magnet, coronal and sagittal multislice images were obtained using a rapid acquisition with relaxation enhancement (RARE) sequence[25] [repetition time (TR)= 4 s, echo train length= 8, echo time (TE)= 60 ms, slice thickness= 1 mm, 7 slices]. The volume of interest (VOI) studied was centered on the striatum (8.2 µl, 1.7 x 2.0 x 2.4 mm³). All first- and second-order shims were adjusted using FASTMAP with echo-planar readout[26]. Localized ^{1}H MR spectra were acquired with a short-echo localization by adiabatic selective refocusing (LASER) sequence [TE= 15 ms, TR= 5 s, 256 transients][27] combined with VAPOR (variable power RF pulses with optimized relaxation delays) water suppression[28]. Spectra were saved as single scans. Unsuppressed water spectra were acquired from the same VOI for metabolite quantification.

Metabolite quantification

Single shots were eddy current, frequency, and phase corrected using MRspa software (http://www.cmrr.umn.edu/downloads/mrspa/) before averaging. The contributions of individual metabolites to the averaged spectra were quantified using LCModel[29] as described previously[24]. The following metabolites were included in the basis set: alanine (Ala), ascorbate/vitamin C (Asc), aspartate (Asp), glycerophosphocholine (GPC), phosphocholine (PCho), creatine (Cr), phosphocreatine (PCr), gamma-aminobutyric acid (GABA), glucose (Glc), glutamine (Gln), glutamate (Glu), glutathione (GSH), glycine (Gly), *myo*-inositol (Ins), lactate (Lac), *N*-acetylaspartate (NAA), *N*-acetylaspartylglutamate (NAAG), phosphoethanolamine (PE), *scyllo*-inositol (Scyllo), taurine (Tau), and macromolecules (MM). The MM spectra were experimentally obtained from a VOI that covered the striatum using an inversion recovery technique [VOI = 4.7 x 2.1 x 2.7 mm³, TE = 15 ms, TR = 2.0 s, inversion time (TIR) = 675 ms, 400 transients, N = 2]. The model metabolite spectra were generated using density matrix simulations[30] with the MATLAB software (MathWorks) based on previously reported chemical shifts and coupling constants[31,32]. Concentrations with mean Cramér-Rao lower bounds ≤20% in any of the 3 groups were reported[24]. If the correlation between two metabolites was consistently high (correlation coefficient $r < -0.7$), their sum was reported rather than the individual values[24].

Synapse density quantification

Two to three independent coronal brain sections were used for each mouse, containing the dorsal striatum (bregma 0.5–1.1 mm) and were stained with presynaptic VGlut1 or VGlut2 (Millipore, 1:500 and 1:1000 respectively) and postsynaptic PSD95 (Thermofisher, 1:500) markers as described previously[8,9,33]. Secondary antibodies used were goat anti-guinea pig Alexa 488 (VGlut1/2) dilution 1:200 and goat anti-rabbit Alex

594 (PSD95) dilution 1:200 (Invitrogen). At least three mice for each genotype; WT, zQ175 and zQ175:CK2α´(+/-) were evaluated. The confocal scans (optical section depth 0.34 mm, 15 sections per scan) of the synaptic zone in the dorsal striatum were performed at 60X magnification on an Olympus FV1000 confocal laser-scanning microscope. Maximum projections of three consecutive optical sections were generated. The Puncta Analyzer Plugin for ImageJ was used to count co-localized synaptic puncta in a blinded fashion. This assay takes the advantage of the fact that presynaptic and postsynaptic proteins reside in separate cell compartments (axons and dendrites, respectively), and they would appear to co-localize at synapses because of their close proximity. The number of animals used in this analysis was 3 per genotype (3 month timepoint), 4 per genotype (6 month timepoint), and 5-6 WT, 7-8 zQ175, and 3 zQ175:CK2α'$^{(+/-)}$ (12 month timepoint).

Data Analysis

All statistics were conducted using GraphPad Prism 9 software. Group averages between genotypes were compared at each time point using one-way ANOVA for MRS and synapse densities with Tukey's post-hoc test to adjust for multiple comparisons. Linear regression and correlation analyses were run separately for each neurochemical against synapse number and Pearson's coefficient and unadjusted p-values were calculated to establish significant correlations. Holm-Šídák adjustment of p-values was used to correct for the multiple testing of the many neurochemicals. P-values of metabolites and sums were analyzed separately from metabolite ratios. A full report of significant results for MRS ANOVAs are in Table 1, with synapse analyses in Table 2, correlation analyses and adjusted p-values in Table 3. Neurochemical concentrations are presented always as mean ± SD while synapse density is presented always as mean ± SEM.

RESULTS

Longitudinal *in vivo* ^{1}H-MRS captures genotype and age-specific striatal neurochemical changes in the zQ175 HD mouse model

MRS studies have been widely applied to evaluate neurodegeneration in several mouse models of HD and patients with HD[16–20]. The use of mouse models allows for parallel characterization of neurochemical concentrations and neuropathological features, an essential aspect of understanding how different neurochemical abnormalities relate to pathology. We chose the heterozygous knock-in zQ175 HD mouse model (zQ175$^{Tg/0}$) for its slow disease progression and its ability to recapitulate multiple HD-like features observed in patients with HD, such as HTT aggregation, early synaptic deficits, transcriptional dysregulation, gliosis, weight loss, and motor and cognitive impairment[8,17,34].

We utilized *in vivo* ^{1}H-MRS to measure neurochemicals in the striatum of WT, zQ175, and zQ175:CK2α'$^{(+/-)}$ mice in a longitudinal manner (**Fig. 1**). A total of 19 neurochemicals, including 4 sums, were quantified and 4 neurochemical ratios were calculated in the dorsolateral striatum (**Table 1**). Seven neurochemicals (Ala, Asc, Gln, Ins, PE, tCho, and tCr) and three neurochemical ratios (tNAA /tCr, Tau/tCr, and Glu/tCr) showed significant group differences primarily at 6 and 12 months of age (**Fig. 2**). Ala, Asc, Ins, and PE showed an age-dependent decrease in WT mice while Gln increased. Similar age-dependent alterations in brain neurochemicals have also been reported in C57BL/6 mice and in human studies comparing young and middle-aged subjects[35,36], indicating these alterations are common brain modifications during aging.

The levels of several neurochemicals in zQ175 mice significantly differed over time compared to WT. No significant differences in tNAA were observed between WT and zQ175 mice while a higher Ins level in zQ175 mice reached statistical significance only at 6 months (**Fig. 2, Table 1**), recapitulating what was previously reported for this mouse model[17]. Decreased NAA and increased Ins, which are considered markers of neurodegeneration, were previously reported in more severe HD mouse models such as the R6/2 (12 weeks)[16], homozygous zQ175 $^{Tg/Tg}$ (12 months)[18] and in older zQ175 $^{Tg/0}$ (22 months)[16–18,22]. Overall, these data suggest that NAA and Ins may reflect substantial neurodegeneration thus with limited utility to monitor early and progressive neuropathological abnormalities in the zQ175$^{(Tg/0)}$ model.

On the other hand, Gln and tCr were significantly higher and tCho lower in zQ175 mice vs. WT at 6 and 12 months coinciding with previously reported worsening motor and cognitive symptoms. We also found that tNAA/tCr and Tau/tCr were significantly lower in zQ175 than WT mice at 6 and 12 months. While these two ratios were relatively stable in WT mice over time, they showed an age-dependent decrease in zQ175 mice. Overall, changes in Gln, tCr, tCho, tNAA/tCr and Tau/tCr reflect age-dependent changes among WT and zQ175 mice and coincide with symptom onset and progression for this HD mouse model.

Given the previously described positive effects of CK2α' haploinsufficiency in ameliorating HD-like symptoms[8,22], we expected to see a number of neurochemicals that were significantly different between zQ175 and zQ175:CK2α'$^{(+/-)}$ mice. Interestingly, we only observed significant differences between these two genotypes at 3 months for Gln, while no significant differences were observed between WT and zQ175:CK2α'$^{(+/-)}$ mice at any time point, indicating that the characteristic increase in Gln in zQ175 could be delayed as a consequence of manipulating CK2α' levels. zQ175:CK2α'$^{(+/-)}$ mice have previously shown decreased HTT aggregation in the striatum, increased excitatory synaptic transmission and improved motor coordination compared to zQ175[22]. The early lower Gln level in zQ175:CK2α'$^{(+/-)}$ vs. zQ175 mice may therefore reflect those pathological features.

Loss of thalamo-striatal excitatory synapses precedes cortico-striatal synapse loss and is sustained over time

To study whether specific neurochemical alterations relate to changes in synapse density, we first determined changes in excitatory synapse density in our WT, zQ175, and zQ175:CK2α'$^{(+/-)}$ mice, looking at both C-S and T-S circuitries during disease progression (**Fig. 3A**). Synapse density was quantified using immunofluorescent colocalization of the presynaptic markers VGlut1 (Vesicular glutamate transporter 1: specific marker for cortical input) and VGlut2 (Vesicular glutamate transporter 2: specific marker for thalamic input) and the post-synaptic marker PSD-95 (post-synaptic density protein 95) in the dorsolateral striatum of 3, 6, and 12 month old animals (**Fig. 3B**). C-S synapses displayed an initial increase in zQ175:CK2α'$^{(+/-)}$ mice compared to WT, however by 6 months this trend had reversed and by 12 months had become a significant decrease in both zQ175 and zQ175:CK2α'$^{(+/-)}$ mice compared to WT (**Fig. 3C, Table 2**). In contrast, levels of T-S synapses in zQ175 mice were significantly reduced compared to WT at all 3 time points while these decreases were significantly rescued in zQ175:CK2α'$^{(+/-)}$ mice at 3 and 6 months (**Fig. 3D, Table 2**). The lack of statistically significant rescue at 12 months between zQ175 and zQ175:CK2α'$^{(+/-)}$ suggests that CK2α' haploinsufficiency delays the onset of T-S synapse loss but does not prevent progression. Taken together, these data further demonstrate that there are circuit-specific changes in striatal excitatory synapse dysfunction in HD that, in the T-S pathway, are in part ameliorated by reducing levels of CK2α'.

Changes in striatal neurochemical levels correlate with circuit-dependent changes in synapse density

Given the alterations in neurochemical levels and changes in excitatory synapse densities between the different genotypes, we wanted to determine if these two measures were significantly correlated with each other, potentially allowing us to identify surrogate biomarkers for synapse loss in HD. We performed linear regression and correlation analyses across all mice used in this study (n=36). Raw synapse number for each mouse at time of sacrifice was used as the response variable in the analysis and neurochemical levels at the time of sacrifice as the predictor variables (**Fig. 4**, **Table 3**). Regressions were run twice to examine each synaptic circuit, T-S and C-S, and their correlation with each neurochemical level separately.

When analyzed in this manner, we found a significant positive correlation ($p < 0.05$) between C-S synapse number and GABA ($r = 0.5687$, $p = 0.0003$) (**Fig. 4A, B**). Gln ($r = -0.3460$, $p = 0.045$) and tCho ($r = 0.3392$, $p = 0.0497$) also presented a p value <0.05 but due to their low r were not considered to have strong correlation. Holm-Šídák multiple testing adjustment of all p-values to correct type-I error confirmed a significant positive correlation between GABA and C-S synapses. GABA is known for its role as the primary inhibitory neurotransmitter in the adult brain and dysfunction in GABAergic signaling has been implicated in HD mouse models as well as patients with HD[38]. It is important to note that despite the positive correlation between GABA and C-S synapse number, we did not observe a reduction in GABA levels in the two HD models relative to WT (**Table 1**). This is consistent with previous reports that have used ^{1}H-MRS in zQ175 and R6/2 mouse models[16,17]. A potential explanation is that neurochemical

concentrations are presented as the average concentration across multiple mice within the same genotype and the variability obtained did not provide significant changes across different genotypes. However, the correlation analyses are conducted by plotting individual concentrations for each analyzed animal and their corresponding C-S synapse number. This suggests that individual levels of GABA are inherently associated with the C-S synapse density regardless of the genotype.

The Holm-Šídák multiple testing adjusted p-value analysis across all correlations/regressions simultaneously did not reveal any significant results for T-S circuitry. However, when unadjusted p-values for individual linear regression and correlations between synapse number and the different neurochemicals were analyzed, we found multiple significant hits in T-S circuitry with $p<0.05$ (**Table 3**). We found Ala ($r = 0.3993$, $p = 0.0159$), Lac ($r = 0.4072$, $p = 0.0137$), PE ($r = 0.4018$, $p = 0.0151$) and Tau/tCr ($r = 0.4057$, $p = 0.014$) to have the lowest p value and a significant positive correlation (**Table 3, Fig 4C-G**). tCr ($r = -0.3394$, $p = 0.0429$) and tNAA/tCr ($r = 0.3531$, $p = 0.0347$) also presented a p value <0.05 but due to their low r were not considered to have strong correlation. Interestingly, Lac concentration did not show a significant alteration across the different genotypes and Ala was significantly altered only at 6 months between WT and zQ175 (**Table 1**), although both Lac and Ala presented a trend towards reduced levels over time in zQ175 compared with WT mice and were partially increased in zQ175:CK2α'$^{(+/-)}$ (**Table 1**). Similar trends for Ala and Lac were shown in symptomatic R6/2 mice[16]. PE and Tau/tCr were significantly decreased over time in both zQ175 and zQ175:CK2α'$^{(+/-)}$ vs. WT (**Fig. 2, Table 1**). tCr significantly increased over time in both zQ175 and zQ175:CK2α'$^{(+/-)}$ vs. WT (**Fig. 2**) and therefore Tau/tCr could reflect tCr effects. These data indicate that by combining the levels of GABA, Ala, Lac, PE, and Tau/tCr, it could be possible to predict circuit-dependent synapse content during HD.

Discussion

The pathogenic events of many neurodegenerative diseases are triggered by reductions in the number of synapses. Therefore, establishing *in vivo* measures that reflect synapse number would represent a powerful tool in the diagnosis of synaptic changes in numerous brain disorders. In this study, we investigated if non-invasive *in vivo* ^{1}H-MRS reflects excitatory synapse number in the zQ175 mouse model of HD. The combination of longitudinal ^{1}H-MRS and immunofluorescence synapse detection has revealed that distinct neurochemical levels significantly correlated with different striatal glutamatergic synaptic input pathways, suggesting that ^{1}H-MRS could potentially distinguish circuit-dependent synapse changes in HD. To the best of our knowledge, this study is the first to directly assess the longitudinal correlation between neurochemical abnormalities and excitatory synapse density in the mouse brain.

We used a well-established immunofluorescence approach to quantify the number of striatal excitatory synapses from two different synaptic circuits, T-S and C-S, and evaluated their association with different neurochemical levels. Studies using the immunofluorescent synapse assay have previously shown a differential dysregulation of these circuitries in zQ175 mice[8,9]. McKinstry et al., showed that the number of T-S

synapses decreased from P21 to 5 weeks of age while no early changes were observed in C-S synapses[9]. Gomez-Pastor et al., validated the preferential loss of T-S synapses in zQ175 mice[8]. Additional structural and electrophysiological analyses in other mouse models of HD (YAC128 and CAG140) have provided similar results indicating that disruption of T-S synapses preceded depletion of C-S synapses in HD[2,37]. The data presented in this study have validated these previous observations and showed that C-S synapse depletion only occurs at advanced stages of the disease when animals are fully symptomatic while T-S synapse depletion occurs earlier. We also showed that manipulating levels of CK2a', a kinase previously associated with the regulation of synaptic activity[8,22,39], prevented early loss of T-S synapses without altering C-S synapse density, similar to what we previously reported in younger mice[8]. Our data in older mice (12 months) also indicated that manipulating levels of CK2α' does not completely suppress T-S synapse loss but rather delays onset. Although it is unknown how CK2α' haploinsufficiency has a selective effect on early T-S synapse loss, it is possible that its influence is mediated by a different regulatory role between D1-MSNs, which project directly into the substantia nigra, and D2-MSNs, which project indirectly to the substantia nigra via the subthalamic nuclei pathway and are preferentially altered in HD[39,40]. Further studies are warranted to uncover the specific role of CK2α' in the differential regulation of T-S and C-S synapses.

The time-dependent dysregulation of these synaptic circuits in zQ175 mice offered the possibility to determine whether longitudinal neurochemical alterations could be associated with circuit-dependent synaptic loss. ^{1}H-MRS analyses in several mouse models of HD as well as in patients with HD have highlighted key neurochemicals such as NAA, Ins and tCr as biomarkers of neurodegeneration[16–20]. It would be reasonable to hypothesize that some of these neurochemicals could be candidates for monitoring synapse loss. ^{1}H-MRS studies conducted in patients with Spinocerebellar Ataxias (SCA1, SCA2, and SCA6) with different degrees of synapse loss showed a similar ranking in the severity of neurochemical alterations, where Gln, Ins, tCr and tNAA were more dysregulated in patients with SCA2 (characterized with higher synaptic loss) compared to SCA1 or SCA6[13,14]. These results supported the hypothesis that neurochemical abnormalities across different SCAs, and perhaps other neurodegenerative diseases, may reflect abnormalities in synaptic function or density. A recent study in a mouse model of Alzheimer's disease (AD) with engrafted WT neural stem cells (NSC) in the hippocampus followed by ^{1}H-MRS and quantification of synapse density by electron microscopy. The authors showed engrafted NSCs altered the expression of synaptic proteins like PSD-95 and synaptophysin as well as the number of synapses, which paralleled changes in NAA and Glu (Glutamate)[41]. In a different study, ^{1}H-MRS and synaptic protein analyses by immunoblotting in mice fed with a high fat diet showed increases in tCr and Gln paralleled decreased synaptic proteins PSD-95 and VGlut1[42]. These studies used electron microscopy or immunoblotting to quantify synapses, which is highly labor-intensive and not suitable for analysis of diverse individual synapses. In addition, direct correlations between neurochemicals and synapse numbers were not investigated. However, those reports established a plausible connection between key neurochemical alterations and synapse density.

In the case of HD, there are differences between mouse models and patients regarding alterations of specific neurochemicals associated with neurodegeneration, requiring careful analysis and validation of their potential relevance in defining synapse loss. Studies in pre-symptomatic patients with HD indicated that NAA levels were already lower than unaffected individuals and decreased further during disease progression, correlating with impaired motor and cognitive function[43]. However, changes in NAA are mostly observed only in symptomatic HD mice[16–18,44–46]. Similarly, increased myo-inositol (Ins), a glial marker associated with gliosis and astrocyte pathology, is only observed in symptomatic HD mice[16,17,22]. Therefore, NAA and Ins alterations may not be the most appropriate biomarkers to monitor early disease stages in mouse models of HD. Another discrepancy between HD mouse models and patients is striatal tCr levels[47], which are reported to increase in mouse models, but in patients there are controversial and often opposite reports about the directionality of tCr[19,46]. Previous longitudinal MRS analyses performed on a 7T magnet with zQ175 mice did not reveal significant alterations for NAA, Ins or any other neurochemical except for tCr, which showed an increase in older zQ175 (12 months), similar to what we observed[17]. Using a 9.4T scanner, we have validated the absence of progressive changes in NAA or Ins at least up to 12 months of age in zQ175 mice. However, we observed significant alterations in three neurochemicals (Gln, tCho, tCr) and in three neurochemical ratios (tNAA/tCr, Glu/tCr and Tau/tCr) between WT and zQ175 starting at 6 months and progressing at 12 months. We conclude that these neurochemicals are better biomarkers to monitor disease progression in zQ175 mice.

Interestingly among all tested neurochemicals, we only detected a significant alteration in Gln when comparing zQ175 and zQ175:CK2α'$^{(+/-)}$. This was unexpected due to the fact this latest model showed improvements in several HD-like phenotypes including decreased HTT aggregation and astrogliosis, increased synaptic density and neuronal excitability, and improved motor coordination[8,22]. Gln levels increased over time in all mice but were significantly increased in zQ175 compared to WT at 6 and 12 months, consistent with a previously reported excitotoxic state in HD[48,49]. Notably, no significant difference in Gln levels were found between WT and zQ175:CK2α'$^{(+/-)}$. Analyses in R6/2 mice have reported early increases in Gln levels[16]. Increased Gln has been associated with an imbalance in Glu–Gln cycling between neurons and astrocytes, reflecting compromised glutamatergic neurotransmission[50,51]. Therefore it is reasonable to hypothesize that early decreased Gln in zQ175:CK2α'$^{(+/-)}$ vs. zQ175 could be associated with improved neuronal excitability. In support of this hypothesis, we previously showed that AMPA-mediated excitatory transmission in acute dorsolateral striatum coronal slices was significantly improved in zQ175:CK2α'$^{(+/-)}$ compared to zQ175[22]. Since no differences in other progressive neurochemical alterations were observed between zQ175 and zQ175:CK2α'$^{(+/-)}$ we concluded that Gln is better associated with the HD-related features improved by manipulating levels of CK2α'. Additionally, contrary to zQ175 mice, zQ175:CK2α'$^{(+/-)}$ did not show significant alterations for tCho at 12 months between WT and zQ175:CK2α'$^{(+/-)}$. tCho is involved in membrane phospholipid metabolism and its alteration is associated with changes in plasma membrane permeability and maintenance of action potentials, transcellular signaling and vesicular release of neurotransmitters[52,53]. Therefore, decreased alterations in both Gln and tCho

in zQ175:CK2α'$^{(+/-)}$ could contribute to the improved neuronal excitability and synaptic function seen in this mouse model.

In addition, we found a significant positive correlation between levels of GABA and C-S synapse density. Deficiency in GABA signaling has been associated with HD and other movement disorders[38]. Lower GABA content in the dorsal striatum and cortex was reported in postmortem brain tissues from patients with HD[54]. Metabolic profiling using ^{13}C labeling and mass spectrometry in R6/2 mice at a symptomatic stage also showed decreases in GABA synthesis[55]. However, ^{1}H-MRS in the R6/2 model did not reveal changes in GABA levels in symptomatic mice compared with WT[16]. We also failed to detect significant changes in GABA levels between WT and zQ175. The discrepancy between the lack of overall alterations in GABA and its correlation with C-S synapse density can be explained by the fact individual levels of GABA could be inherently associated with the C-S synapse density regardless of genotype. On the other hand, we observed significant correlations between T-S synapse density and Ala, Lac, PE, and Tau/tCr. Studies of amino acid metabolism in patients with HD have shown a decrease in levels of Ala and other neutral amino acids in HD plasma which correlates with symptom status[56,57]. Lac is an end-product of glycolysis associated with brain activity and is taken up by neurons during episodes of glutamatergic synaptic activity[58]. ^{14}C-Lac radiolabeling and uptake/transport analyses in cell models of HD have shown a decrease in Lac uptake in HD cells[58]. However, there is much controversy among ^{1}H-MRS studies about whether Lac is significantly altered in patients[46]. Although not statistically significant, we observed an overall decrease of Ala and Lac in zQ175 over time that was partially rescued in zQ175:CK2α'$^{(+/-)}$. Alterations in PE, tCr and Tau, which are neurochemicals connected with neuronal integrity and function, have been consistently reported in mouse models of HD and patients with HD and are associated with disease burden[16,19,20,46]. We found that Tau/tCr significantly decreased over time in zQ175 and zQ175:CK2α'$^{(+/-)}$ compared with WT and significantly correlated with T-S synapse density. Tau is the second most abundant amino acid in the brain and has neuroprotective functions[59]. Therefore, a decrease in Tau/tCr in HD mice can be interpreted as increased neuronal pathology, which relates to the loss of synapses. Our data indicate that while Gln is a better biomarker to assess disease symptoms and progression, a combination of the levels between GABA, Ala, Lac, PE, and Tau/tCr could be used to predict levels of striatal glutamatergic synapses in HD.

Overall, this study demonstrates the feasibility of using ^{1}H-MRS to monitor synaptic changes *in vivo* during HD progression. While further studies are needed to corroborate these findings in alternative models of HD and other neurodegenerative diseases, this study shows that neurochemical biomarkers that parallel changes in synapse number can be used as a tool to monitor synaptic changes in future pre-clinical trials with HD models.

Acknowledgements: We thank Dr. Dinesh Deelchand for guidance in data analysis and assistance in LCModel basis set generation.

Authors' Roles: R.G.P. and G. O. obtained funding for this study and designed the experiments. N.Z., K.G., J.C., and D.Y. performed the experiments. N.Z., K.G., J.C.,

and D.Y. prepared and analyzed the data. G.O. supervised the MRS data acquisition and analysis. R.G.P. supervised the *ex vivo* tissue collection and synapse analyses. L.E. supervised the statistical analyses. N.Z. and R.G.P. wrote the first draft of the manuscript and all authors edited subsequent versions and approved the final version of the manuscript.

Financial Disclosure: Nothing to report.

Figure and Table legends (40 words)

Figure 1. **Localized proton MR spectra measured from the mouse dorsolateral striatum. A**) WT **B**) zQ175$^{(Tg/0)}$ and **C**) zQ175$^{(Tg/0)}$:CK2α'$^{(+/-)}$ mice at 3, 6, and 12 months old. The volume of interest is shown on T2-weighted images and alterations in neurochemicals visible in the spectra are shown.

Figure 2. **Age and genotype-dependent neurochemical alterations in the mouse dorsolateral striatum**. Longitudinal metabolite profile in WT, zQ175, and zQ175:CK2α'$^{(+/-)}$ mice. Only neurochemicals that showed significant differences between genotypes are shown (see Table 1). Error bars represent mean ± SD. One-way ANOVA with Tukey's post-hoc test. *p<0.05 WT vs. zQ175, # p<0.05 WT vs. zQ175:CK2α'$^{(+/-)}$, ♦ p<0.05 zQ175 vs. zQ175:CK2α'$^{(+/-)}$. Abbreviation explanations can be found in the methods section. For 3 month WT n=13, zQ175 n= 16, zQ175:CK2α'$^{(+/-)}$ n=18. 6 month WT n=9, zQ175 n= 12, zQ175:CK2α'$^{(+/-)}$ n=13. 12 month WT n=5, zQ175 n= 8, zQ175:CK2α'$^{(+/-)}$ n=7.

Figure 3. **Onset of thalamo-striatal (T-S) synapse loss precedes cortico-striatal synapse deficits in zQ175 mice and it is delayed in zQ175:CK2α'$^{(+/-)}$ mice. A**) Diagram of the striatal excitatory circuitry. **B**) Colocalization (white arrows) of pre-synaptic (VGlut1/2) and post-synaptic (PSD-95) markers in WT, zQ175, and zQ175:CK2α'$^{(+/-)}$ mice. Representative images from 6 months. Scale bar: 5 μm. **C-D**) Quantification of C-S and T-S synapses respectively at 3, 6, and 12 months old between genotypes. Error bars represent mean ± SEM. *p<0.05, **p<0.01, ***p<0.001, ****p<0.0001, one-way ANOVA with Tukey's post-hoc test. At each time point, WT n= 3-6, zQ175 n= 3-8, zQ175:CK2α'$^{(+/-)}$ n=3-4.

Figure 4. **Selective neurochemical alterations differentially correlate with striatal synaptic circuits**. **A**) Illustration of C-S correlation with metabolites (GABA). **B**) Correlation analysis of C-S synapse density vs. GABA where raw synapse numbers are plotted against corresponding neurochemical levels. **C**) illustration T-S correlation with metabolites. **D-G**) correlation analysis of neurochemicals vs T-S synapse density. r value represents Pearson's correlation. WT n=12, zQ175 n=15, zQ175:CK2α'$^{(+/-)}$ n=9.

Table 1. **Longitudinal neurochemical concentrations measured by ^{1}H-MRS.** Neurochemical concentrations in WT, zQ175, and zQ175:CK2α'$^{(+/-)}$ mice over time. Values represented as mean ± SD. One-way ANOVA with Tukey's post-hoc test. * indicates WT vs. zQ175, # indicates WT vs. zQ175:CK2α'$^{(+/-)}$, and ♦ indicates zQ175 vs. zQ175:CK2α'$^{(+/-)}$.

Table 2. **Synapse density analyses in C-S and T-S circuitries.** Mean synapse density (relative to WT) between genotypes and across time points. Error presented as SEM. One-way ANOVA with Tukey's post-hoc test.

Table 3. **Correlation analyses between synapse number and metabolite concentration.** Pearson's coefficient and unadjusted p-value calculated from correlation analyses between all neurochemicals and synapse # (C-S and T-S correlations run separately). Holm-Šídák multiple comparison post-hoc test was run for C-S and T-S separately, represented by adjusted p-values. All ages and genotypes are pooled for each analysis.

References

1. MacDonald ME, Ambrose CM, Duyao MP, et al. A novel gene containing a trinucleotide repeat that is expanded and unstable on Huntington's disease chromosomes. *Cell* 1993; **72**: 971-983.

2. Raymond LA, André VM, Cepeda C, Gladding CM, Milnerwood AJ, Levine MS. Pathophysiology of Huntington's disease: Time-dependent alterations in synaptic and receptor function. *Neuroscience* 2011; **198**: 252-273.

3. Unschuld PG, Joel SE, Liu X, et al. Impaired cortico-striatal functional connectivity in prodromal Huntington's Disease. *Neurosci Lett* 2012; **514**: 204-209.

4. Huerta-Ocampo I, Mena-Segovia J, Bolam JP. Convergence of cortical and thalamic input to direct and indirect pathway medium spiny neurons in the striatum. *Brain Struct Funct* 2014; **219**: 1787-1800.

5. Smith Y, Raju D, Nanda B, Pare J-F, Galvan A, Wichmann T. The Thalamostriatal Systems: Anatomical and Functional Organization in Normal and Parkinsonian States. *Brain Res Bull* 2009; **78**: 60-68.

6. Cepeda C, Wu N, André VM, Cummings DM, Levine MS. The Corticostriatal Pathway in Huntington's Disease. *Prog Neurobiol* 2007; **81**: 253-271.

7. Kolodziejczyk K, Raymond LA. Differential changes in thalamic and cortical excitatory synapses onto striatal spiny projection neurons in a Huntington disease mouse model. *Neurobiol Dis* 2016; **86**: 62-74.

8. Gomez-Pastor R, Burchfiel ET, Neef DW, et al. Abnormal degradation of the neuronal stress-protective transcription factor HSF1 in Huntington's disease. *Nat Commun* 2017; **8**.

9. Mckinstry SU, Karadeniz YB, Worthington AK, et al. Huntingtin Is Required for Normal Excitatory Synapse Development in Cortical and Striatal Circuits. *Neurobiol Dis* 2014; **34**: 9455-9472.

10. Finnema SJ, Nabulsi NB, Eid T, et al. Imaging synaptic density in the living human brain. *Sci Transl Med* 2016; **8**.

11. Thomsen MB, Jacobsen J, Lillethorup TP, et al. In vivo imaging of synaptic SV2A protein density in healthy and striatal-lesioned rats with [11C]UCB-J PET. *J Cereb Blood Flow Metab* 2021; **41**: 819-830.

12. Oz G, Nelson CD, Koski DM, et al. Noninvasive detection of presymptomatic and progressive neurodegeneration in a mouse model of spinocerebellar ataxia type 1. *J Neurosci* 2010; **30**: 3831-3838.

13. Öz G, Vollmers ML, Nelson CD, et al. In vivo monitoring of recovery from

neurodegeneration in conditional transgenic SCA1 mice. *Exp Neurol* 2011; **232**: 290-298.

14. Joers JM, Deelchand DK, Lyu T, et al. Neurochemical abnormalities in premanifest and early spinocerebellar ataxias. *Ann Neurol* 2018; **83**: 816-829.

15. *Magnetic Resonance Spectroscopy of Degenerative Brain Diseases*. Springer International Publishing 2016.

16. Tkáč I, Dubinsky JM, Keene CD, Gruetter R, Low WC. Neurochemical changes in Huntington R6/2 mouse striatum detected by in vivo1H NMR spectroscopy. *J Neurochem* 2007; **100**: 1397-1406.

17. Heikkinen T, Lehtimäki K, Vartiainen N, et al. Characterization of Neurophysiological and Behavioral Changes, MRI Brain Volumetry and 1H MRS in zQ175 Knock-In Mouse Model of Huntington's Disease. Okazawa H, ed. *PLoS One* 2012; **7**.

18. Peng Q, Wu B, Jiang M, et al. Characterization of Behavioral, Neuropathological, Brain Metabolic and Key Molecular Changes in zQ175 Knock-In Mouse Model of Huntington's Disease. *PLoS One* 2016; **11**.

19. Sturrock A, Laule C, Wyper K, et al. A Longitudinal Study of Magnetic Resonance Spectroscopy Huntington's Disease Biomarkers. *Mov Disord* 2015; **30**.

20. Sturrock A, Laule C, Decolongon J, et al. Magnetic resonance spectroscopy biomarkers in premanifest and early Huntington disease. *Neurology* 2010; **75**: 1702-1710.

21. Öz G, Iltis I, Hutter D, Thomas W, Bushara KO, Gomez CM. Distinct Neurochemical Profiles of Spinocerebellar Ataxias 1, 2, 6, and Cerebellar Multiple System Atrophy. *Cerebellum* 2011; **10**: 208-217.

22. Yu D, Zarate N, Cuccu F, et al. Protein kinase CK2 alpha prime and alpha-synuclein constitute a key regulatory pathway in Huntington's disease. *bioRxiv* 2020. doi:10.1101/2020.10.29.359380

23. Öz G, Kittelson E, Demirgoz D, et al. Assessing recovery from neurodegeneration in spinocerebellar ataxia 1: COMPARISON of in vivo magnetic resonance spectroscopy with motor testing, gene expression and histology. *Neurobiol Dis* 2015; **74**: 158-166.

24. Friedrich J, Kordasiewicz HB, O'Callaghan B, et al. Antisense oligonucleotide–mediated ataxin-1 reduction prolongs survival in SCA1 mice and reveals disease-associated transcriptome profiles. *JCI Insight* 2018; **3**.

25. Hennig J, Nauerth A, Friedburg H. RARE imaging: A fast imaging method for clinical MR. *Magn Reson Med* 1986; **3**: 823-833.

26. Gruetter R, Tkáč I. Field Mapping Without Reference Scan Using Asymmetric Echo-Planar Techniques. *Magn Reson Med* 2000; **43**: 319-323.

27. Garwood M, DelaBarre L. The Return of the Frequency Sweep: Designing Adiabatic Pulses for Contemporary NMR. *J Magn Reson* 2001; **153**: 155-177.

28. Tkáč I, Starčuk Z, Choi I-Y, Gruetter R. In Vivo 1 H NMR Spectroscopy of Rat Brain at 1 ms Echo Time. *Magn Reson Med* 1999; **41**: 649-656.

29. Provencher SW. Estimation of metabolite concentrations from localized in vivo proton NMR spectra. *Magn Reson Med* 1993; **30**: 672-679.

30. Deelchand DK, Henry P-G, Uğurbil K, Marjańska M. Measurement of transverse relaxation times of J-coupled metabolites in the human visual cortex at 4 T. *Magn Reson Med* 2012; **67**: 891-897.

31. Govindaraju V, Young K, Maudsley AA. Proton NMR chemical shifts and coupling constants for brain metabolites. *NMR Biomed* 2000; **13**: 129-153.

32. Tkáč I. Refinement of simulated basis set for LCModel analysis. In: *16th Annual Meeting ISMRM*.; 2008: 1624.

33. Ippolito DM, Eroglu C. Quantifying synapses: An immunocytochemistry-based assay to quantify synapse number. *J Vis Exp* 2010.

34. Menalled LB, Kudwa AE, Miller S, et al. Comprehensive Behavioral and Molecular Characterization of a New Knock-In Mouse Model of Huntington's Disease: zQ175. *PLoS One* 2012; **7.**

35. Duarte JMN, Do KQ, Gruetter R. Longitudinal neurochemical modifications in the aging mouse brain measured in vivo by 1H magnetic resonance spectroscopy. *Neurobiol Aging* 2014; **35**: 1660-1668.

36. Grachev ID, Apkarian AV. Aging alters regional multichemical profile of the human brain: an in vivo1H-MRS study of young versus middle-aged subjects. *J Neurochem* 2001; **76**: 582-593.

37. Deng YP, Wong T, Wan JY, Reiner A. Differential loss of thalamostriatal and corticostriatal input to striatal projection neuron types prior to overt motor symptoms in the Q140 knock-in mouse model of Huntington's disease. *Front Syst Neurosci* 2014; **8.**

38. Hsu Y-T, Chang Y-G, Chern Y. Insights into GABAAergic system alteration in Huntington's disease. *Open Biol* 2018; **8**.

39. Rebholz H, Zhou M, Nairn AC, Greengard P, Flajolet M. Selective Knockout of the Casein Kinase 2 in D1 Medium Spiny Neurons Controls Dopaminergic Function. *Biol Psychiatry* 2013; **74**: 113-121.

40. Reiner A, Albin RL, Anderson KD, D'Amato CJ, Penney JB, Young AB. Differential loss of striatal projection neurons in Huntington disease. *Proc Natl Acad Sci U S A* 1988; **85**: 5733-5737.

41. Zhang W, Gu G-J, Zhang Q, et al. NSCs promote hippocampal neurogenesis, metabolic changes and synaptogenesis in APP/PS1 transgenic mice. *Hippocampus* 2017; **27**: 1250-1263.

42. Lizarbe B, Soares AF, Larsson S, Duarte JMN. Neurochemical Modifications in the Hippocampus, Cortex and Hypothalamus of Mice Exposed to Long-Term High-Fat Diet. *Front Neurosci* 2018; **12**.

43. Leavitt BR, Weir DW, Sturrock A. Development of biomarkers for Huntington's disease. *Lancet Neurol* 2011; **10**: 573-590.

44. Pépin J, Francelle L, Carrillo-de Sauvage MA, et al. In vivo imaging of brain glutamate defects in a knock-in mouse model of Huntington's disease. *Neuroimage* 2016; **139**: 53-64.

45. Tkáč I, Henry P-G, Zacharoff L, et al. Homeostatic Adaptations in Brain Energy Metabolism in Mouse Models of Huntington Disease. *J Cereb Blood Flow Metab* 2012; **32**: 1977-1988.

46. Adanyeguh IM, Monin M-L, Rinaldi D, et al. Expanded neurochemical profile in the early stage of Huntington disease using proton magnetic resonance spectroscopy. *NMR Biomed* 2018; **31**.

47. Sánchez-Pernaute R, García-Segura JM, Del Barrio Alba A, Viaño J, De Yébenes JG. Clinical correlation of striatal 1H MRS changes in Huntington's disease. *Neurology* 1999; **53**: 806-812.

48. Fan MMY, Raymond LA. N-methyl-D-aspartate (NMDA) receptor function and excitotoxicity in Huntington's disease. *Prog Neurobiol* 2007; **81**: 272-293.

49. Hassel B, Tessler S, Faull RLM, Emson PC. Glutamate uptake is reduced in prefrontal cortex in Huntington's disease. *Neurochem Res* 2008; **33**: 232-237.

50. Liévens JC, Woodman B, Mahal A, et al. Impaired glutamate uptake in the R6 Huntington's disease transgenic mice. *Neurobiol Dis* 2001; **8**: 807-821.

51. Behrens PF, Franz P, Woodman B, Lindenberg KS, Landwehrmeyer GB. Impaired glutamate transport and glutamate–glutamine cycling: downstream effects of the Huntington mutation. *Brain* 2002; **125**: 1908-1922.

52. Aureli M, Grassi S, Prioni S, Sonnino S, Prinetti A. Lipid membrane domains in the brain. *Biochim Biophys Acta* 2015; **1851**: 1006-1016.

53. Lauwers E, Goodchild R, Verstreken P. Membrane Lipids in Presynaptic Function

and Disease. *Neuron* 2016; **90**: 11-25.

54. Spokes EGS, Garrett NJ, Rossor MN, Iversen LL. Distribution of GABA in post-mortem brain tissue from control, psychotic and Huntington's chorea subjects. *J Neurol Sci* 1980; **48**: 303-313.

55. Skotte NH, Andersen J V., Santos A, et al. Integrative Characterization of the R6/2 Mouse Model of Huntington's Disease Reveals Dysfunctional Astrocyte Metabolism. *Cell Rep* 2018; **23**: 2211-2224.

56. Reilmann R, Rolf LH, Lange HW. Decreased plasma alanine and isoleucine in Huntington's disease. *Acta Neurol Scand* 1995; **91**: 222-224.

57. Underwood BR, Broadhurst D, Dunn WB, et al. Huntington disease patients and transgenic mice have similar pro-catabolic serum metabolite profiles. *Brain* 2006; **129**: 877-886.

58. Solís-Maldonado M, Miró MP, Acuña AI, et al. Altered lactate metabolism in Huntington's disease is dependent on GLUT3 expression. *CNS Neurosci Ther* 2018; **24**: 343-352.

59. Kim, H, Kim, H, Yoon, J, et al. Taurine in drinking water recovers learning and memory in the adult APP/PS1 mouse model of Alzheimer's disease. *Sci Rep* 2014; **4**.

Table 1. **Longitudinal neurochemical concentrations measured by ^{1}H-MRS.**

µmol/g ± SD												
	3 Months				6 Months				12 Months			
Metabolite	**WT**	**zQ175**	**zQ175:CK2α'$^{(+/-)}$**	**P value**	**WT**	**zQ175**	**zQ175:CK2α'$^{(+/-)}$**	**P value**	**WT**	**zQ175**	**zQ175:CK2α'$^{(+/-)}$**	**P value**
Ala	1.64 ± 0.31	1.5 ± 0.29	1.5 ± 0.37	ns	1.21 ± 0.24	0.89 ± 0.21	1.06 ± 0.22	**0.0071	0.97 ± 0.33	0.81 ± 0.32	0.90 ± 0.09	ns
Asc	1.33 ± 0.27	1.32 ± 0.20	1.28 ± 0.30	ns	1.30 ± 0.26	1.44 ± 0.36	1.52 ± 0.26	ns	1.10 ± 0.24	1.45 ± 0.44	1.74 ± 0.45	#0.0389
Asp	n/a	1.52 ± 0.46	1.39 ± 0.28	ns	1.56 ± 0.49	1.46 ± 0.41	1.57 ± 0.38	ns	n/a	1.60 ± 0.31	n/a	ns
GABA	2.59 ± 0.41	2.69 ± 0.26	2.74 ± 0.30	ns	2.49 ± 0.26	2.59 ± 0.27	2.59 ± 0.28	ns	2.48 ± 0.14	2.40 ± 0.29	2.43 ± 0.37	ns
Glc	2.49 ± 1.04	n/a	2.24 ± 0.89	ns	2.68 ± 0.60	2.87 ± 0.96	1.72 ± 0.63	#0.0228 ◆◆0.0019	n/a	n/a	n/a	ns
Gln	2.95 ± 0.20	3.16 ± 0.15	2.87 ± 0.26	*0.0259 ◆ ◆ ◆ 0.0009	3.06 ± 0.10	3.36 ± 0.24	3.21 ± 0.27	* 0.0143	3.46 ± 0.25	4.12 ± 0.35	3.79 ± 0.26	**0.0031
Glu	6.86 ± 0.51	7.07 ± 0.40	6.82 ± 0.45	ns	7.01 ± 0.54	7.11 ± 0.30	7.04 ± 0.51	ns	7.24 ± 0.46	7.06 ± 0.60	7.15 ± 0.23	ns
GSH	0.98 ± 0.08	0.99 ± 0.11	1.04 ± 0.12	ns	1.11 ± 0.16	1.00 ± 0.16	0.96 ± 0.13	ns	0.88 ± 0.10	0.78 ± 0.27	0.87 ± 0.15	ns
Gly	1.01 ± 0.17	0.94 ± 0.24	1.04 ± 0.13	ns	1.00 ± 0.15	1.12 ± 0.17	1.09 ± 0.25	ns	0.84 ± 0.27	1.05 ± 0.32	1.11 ± 0.25	ns
Ins	3.70 ± 0.36	4.10 ± 0.52	3.95 ± 0.41	ns	3.72 ± 0.32	4.24 ± 0.49	4.16 ± 0.24	**0.0076 #0.0234	3.41 ± 0.38	3.89 ± 0.48	3.98 ± 0.39	ns
Lac	6.54 ± 0.96	6.21 ± 0.86	6.48 ± 1.00	ns	5.56 ± 1.36	5.02 ± 0.93	5.60 ± 0.69	ns	5.50 ± 1.63	4.76 ± 1.46	5.06 ± 0.85	ns
Mac	128.80 ± 5.18	127.31 ± 4.54	125.85 ± 4.01	ns	122.73 ± 4.60	127.41 ± 6.41	125.43 ± 6.21	ns	126.68 ± 4.05	124.57 ± 2.37	124.71 ± 5.07	ns
NAA	6.15 ± 0.19	6.11 ± 0.18	6.05 ± 0.23	ns	6.13 ± 0.16	6.13 ± 0.21	6.01 ± 0.21	ns	6.36 ± 0.23	6.10 ± 0.31	6.03 ± 0.41	ns
PE	2.64 ± 0.42	2.60 ± 0.41	2.54 ± 0.23	ns	2.61 ± 0.34	2.13 ± 0.42	2.17 ± 0.30	* 0.0129 # 0.0218	2.25 ± 0.21	2.17 ± 0.15	2.04 ± 0.30	ns
Tau	13.47 ± 1.14	13.02 ± 0.79	13.01 ± 0.73	ns	12.87 ± 0.42	12.34 ± 0.92	12.14 ± 0.60	ns	13.08 ± 1.16	12.31 ± 1.27	12.56 ± 0.76	ns
tCho	1.47 ± 0.13	1.4 ± 0.11	1.32 ± 0.08	##0.0027	1.54 ± 0.12	1.39 ± 0.14	1.31 ± 0.10	* 0.0242 ### 0.0005	1.51± 0.04	1.32 ± 0.16	1.34 ± 0.09	*0.0354
tCr	7.54 ± 0.22	7.62 ± 0.19	7.55 ± 0.20	ns	7.71 ± 0.35	8.35 ± 0.25	8.17 ± 0.24	****<0.0001 ##0.0015	7.54 ± 0.32	8.48 ± 0.63	8.52 ± 0.31	**0.0076 ##0.0069
NAA+NAAG	6.39 ± 0.22	6.34 ± 0.18	6.32 ± 0.27	ns	6.39 ± 0.18	6.34 ± 0.24	6.26 ± 0.28	ns	6.62 ± 0.28	6.38 ± 0.28	6.26 ± 0.43	ns
Glc+Tau	15.76 ± 2.16	15.41 ± 1.48	15.25 ± 1.22	ns	15.25 ± 0.93	15.22 ± 1.63	13.86 ± 0.88	#0.0340 ◆0.0239	14.78 ± 1.98	14.60 ± 2.31	14.00 ± 1.48	ns
tNAA/tCr	0.85 ± 0.03	0.83 ± 0.03	0.84 ± 0.03	ns	0.83 ± 0.04	0.76 ± 0.03	0.77 ± 0.03	***0.0002 ## 0.0005	0.88 ± 0.04	0.75 ± 0.06	0.74 ± 0.06	**0.0047 ##0.0018
Glu/tCr	0.91 ± 0.06	0.93 ± 0.05	0.90 ± 0.06	ns	0.91 ± 0.08	0.85 ± 0.03	0.86 ± 0.07	ns	0.96 ± 0.07	0.83 ± 0.07	0.84 ± 0.06	**0.0081 #0.0145
Tau/tCr	1.78 ± 0.13	1.71 ± 0.10	1.72 ± 0.09	ns	1.67 ± 0.08	1.48 ± 0.10	1.49 ± 0.05	****<0.0001 ####<0.0001	1.73 ± 0.12	1.45 ± 0.09	1.47 ± 0.08	***0.0003 ###0.0008
Glu/Ins	1.87 ± 0.18	1.75 ± 0.21	1.75 ± 0.24	ns	1.90 ± 0.23	1.70 ± 0.22	1.70 ± 0.16	ns	2.12 ± 0.11	1.81 ± 0.29	1.80 ± 0.23	ns

Table 2. Synapse density analyses in C-S and T-S circuitries.

C-S Synapses						
	3 months		6 Months		12 Months	
	Mean (% of WT)	Adjusted p-value	Mean (% of WT)	Adjusted p-value	Mean (% of WT)	Adjusted p-value
WT vs zQ175	100.00 ± 7.76 vs 110.90 ± 6.39	0.5769	100.00 ± 6.31 vs 86.59 ± 5.10	0.1976	100.00 ± 5.11 vs 60.91 ± 2.34	<0.0001
WT vs zQ175:CK2α′$^{(+/-)}$	100.00 ± 7.76 vs 135.8.0 ± 8.25	0.0031	100.00 ± 6.31 vs 81.09 ± 4.79	0.0425	100.00 ± 5.11 vs 68.34 ± 4.37	<0.0001
zQ175 vs zQ175:CK2α′$^{(+/-)}$	110.90 ± 6.39 vs 135.80 ± 8.25	0.0628	86.59 ± 5.10 vs 81.09 ± 4.79	0.7661	60.91 ± 2.34 vs 68.34 ± 4.37	0.4883
T-S Synapses						
	3 months		6 Months		12 Months	
	Mean (% of WT)	Adjusted p-value	Mean (% of WT)	Adjusted p-value	Mean (% of WT)	Adjusted p-value
WT vs zQ175	100.00 ± 5.85 vs 79.04 ± 4.52	0.0134	100.00 ± 7.74 vs 62.17 ± 6.92	0.013	100.00 ± 6.29 vs 73.23 ± 3.29	0.006
WT vs zQ175:CK2α′$^{(+/-)}$	100.00 ± 5.85 vs 101.50 ± 4.79	0.9778	100.00 ± 7.74 vs 115.60 ± 13.02	0.4771	100.00 ± 6.29 vs 89.20 ± 15.09	0.5932
zQ175 vs zQ175:CK2α′$^{(+/-)}$	79.04 ± 4.52 vs 101.50 ± 4.79	0.0083	62.17 ± 6.92 vs 115.60 ± 13.02	0.0004	73.23 ± 3.29 vs 89.20 ± 15.09	0.29

Table 3. Correlation analyses between synapse number and metabolite concentration

	T-S Synapse #			C-S Synapse #		
Metabolite	Pearson's r	Unadjusted p-value	Adjusted p-value	Pearson's r	Unadjusted p-value	Adjusted p-value
Ala	0.3993	0.0159	0.2396	-0.07708	0.6648	0.9969
Asc	0.1352	0.4316	0.9872	-0.1922	0.2762	0.9793
Asp	-0.2735	0.1065	0.7411	0.1269	0.4745	0.9969
GABA	-0.1916	0.263	0.9527	0.5867	0.0003	0.0057
Glc	-0.1248	0.4684	0.9872	0.2246	0.2015	0.9658
Gln	-0.007744	0.9642	0.9872	-0.346	0.045	0.5634
Glu	-0.291	0.0851	0.7252	0.09244	0.6031	0.9969
GSH	-0.1381	0.4219	0.9872	0.2216	0.2078	0.9658
Gly	-0.2817	0.096	0.7307	0.1223	0.4907	0.9969
Ins	-0.2933	0.0825	0.7252	0.08881	0.6174	0.9969
Lac	0.4072	0.0137	0.2306	-0.2056	0.2435	0.9734
Mac	0.1318	0.4437	0.9872	0.1108	0.5328	0.9969
NAA	0.03198	0.8531	0.9872	0.1599	0.3662	0.9895
PE	0.4018	0.0151	0.2396	-0.04997	0.779	0.9969
Tau	0.2471	0.1462	0.8242	0.1849	0.2951	0.9793
tCho	-0.1602	0.3506	0.9795	0.3392	0.0497	0.5796
tCr	-0.3394	0.0429	0.5042	-0.1056	0.5523	0.9969
tNAA (NAA+NAAG)	0.1387	0.4198	0.9872	0.07763	0.6626	0.9969
Glc+Tau	0.05664	0.7428	0.9872	0.2565	0.1431	0.9155
tNAA/tCr	0.3531	0.0347	0.1005	0.1401	0.4295	0.6745
Glu/tCr	0.06251	0.7172	0.8027	0.1992	0.2586	0.6348
Tau/tCr	0.4057	0.0141	0.0552	0.2147	0.2226	0.6348
Glu/Ins	0.1015	0.5558	0.8027	-0.04812	0.787	0.787

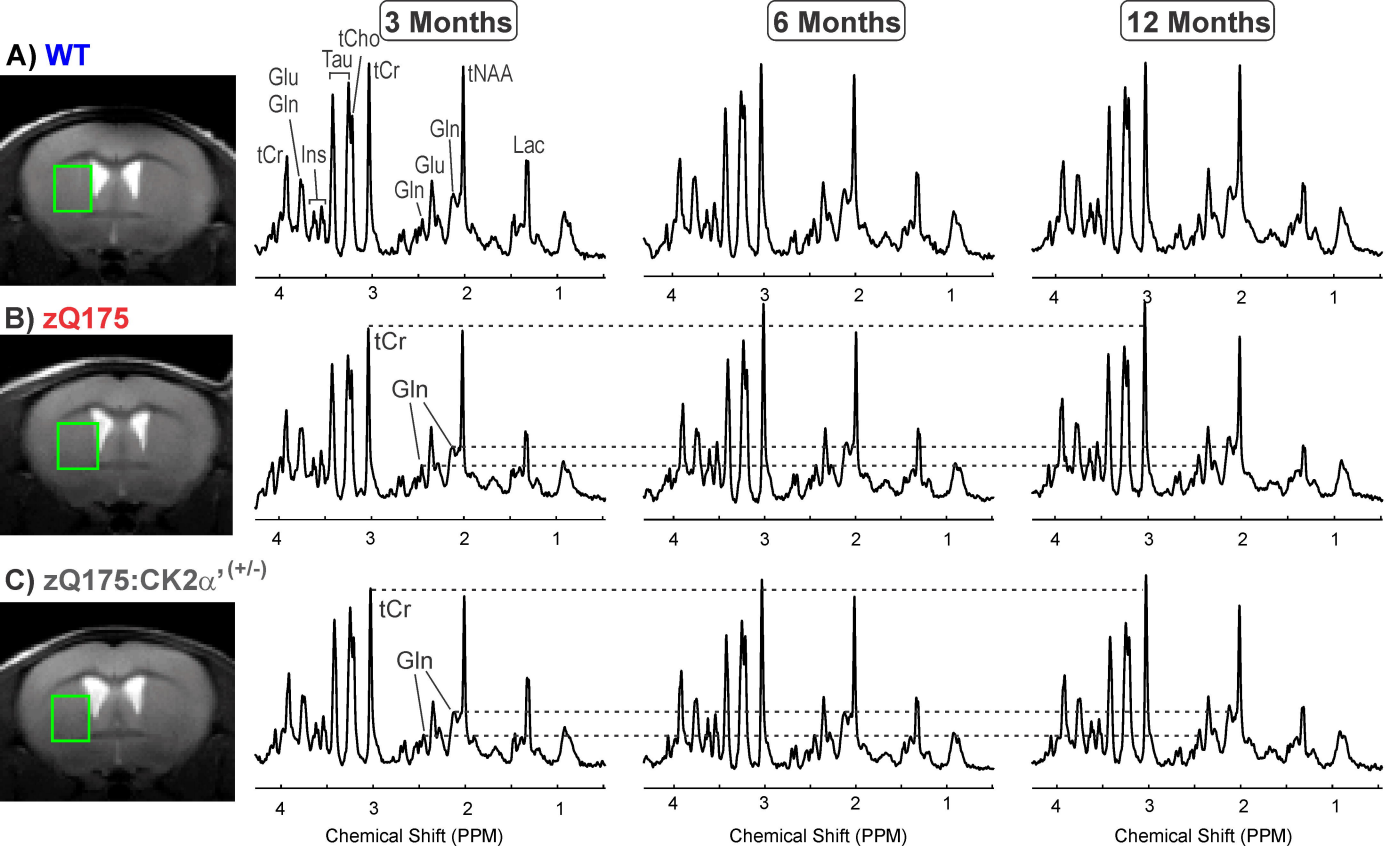
3 Months
6 Months
12 Months
A) WT
B) zQ175
C) zQ175:CK2α'(+/-)
tCho
Tau
tCr
tNAA
Glu
Gln
Ins
Lac
Chemical Shift (PPM)
Chemical Shift (PPM)
Chemical Shift (PPM)